JOURNAL OF AIRCRAFT
Vol. 41, No. 4, July–August 2004

Hypersonic Power-Law Shaped Waveriders in Off-Design Regimes

I. I. Mazhul* and R. D. Rakchimov†
Russian Academy of Science, 630090, Novosibirsk, Russia

Waveriders with lower surfaces defined by power-law functions have been generated based on the flow behind planar oblique shock waves. Results of numerical simulation of the inviscid three-dimensional steady-state flow near the waveriders in off-design regimes are presented. A finite volume method is used to solve the Euler equations. The features of gasdynamic flow patterns near a compression surface are investigated with particular attention to the possibility to design configurations flown without inner shocks at regimes of freestream Mach numbers larger than the design Mach values. The results were obtained at the freestream Mach numbers of 4, 5, 6, 6.5, and 8 and angles of attack up to 21 deg. The design Mach numbers of the waveriders studied are 4, 6, and 7.

Nomenclature

A, B	=	power-law parameters
C_p	=	pressure coefficient, $(p - p_\infty)/q_\infty$
L	=	waverider length, m
l	=	waverider span, m
M	=	flow Mach number
n	=	power-law exponent
p	=	local static pressure, N/m^2
p/p_∞	=	relative static pressure
q_∞	=	freestream dynamic pressure, N/m^2
S_{pl}	=	planform area of waverider, m^2
x, y, z	=	coordinate axes, see Fig. 1
$\bar{x}$, $\bar{z}$	=	relative longitudinal and transversal coordinates, x/L and $2z/l$
α	=	angle of attack, deg
β	=	oblique shock wave inclination angle, deg
δ	=	basic-wedge angle, deg
λ	=	aspect ratio, l^2/S_{pl}
ρ/ρ_∞	=	relative density

Subscripts

d	=	design regimes
l	=	lower surface
u	=	upper surface
pl	=	planform
∞	=	freestream values

Introduction

WAVERIDERS are aerodynamic configurations whose design is based on known supersonic and hypersonic flowfields with given properties. Waverider lower surfaces have been generated by use of the flow streamlines behind planar oblique shocks, for example, in Refs. 1–3, behind conical shock waves around circular or elliptical cones,[5,6] and power-law shocks,[7–9] as well as the flows in converging cone ducts[10] and some others.

Investigations have shown that it is possible to design waveriders with the same features that may be advantageous for hypersonic configurations. Therefore, in addition to investigations of waveriders, the possibilities to use waveriders for design of hypersonic scramjet-powered vehicle configurations have recently been considered.[11–16] This allows one to obtain reliable estimations of aerodynamic loads in on-design flow regimes and, evidently, to obtain higher values of lift-to-drag ratios. On the other hand, a proper choice of the basic flow may ensure necessary uniformity of the flowfield in the front of the engine inlet located under the waverider lower surface. Moreover, because the shock wave in the on-design regime is attached to the leading edges and there is no spillage from the lower surface to the upper surface, higher flow compression can be realized ahead the inlet as compared with other spatial configurations.

Waverider-based hypersonic vehicles must operate in a wide range of freestream Mach numbers, not only in the on-design regime. When the freestream Mach numbers M_∞ are larger than the design value M_d of the configuration design, the shock wave is located above the plane of the leading edges, and a complex system of intersecting shocks can form. When these shocks hit the inlet, this can lead to a noticeable nonuniformity of the flow in the engine channel and a decrease of efficiency of the power plant on the whole. In addition, when they descend to a body surface or inlet lip, they can cause local separations of the boundary layer and peaks of the heat fluxes. Therefore, it is necessary to investigate the off-design regimes of the waveriders to clear up the flow characteristics and possible structure of the shock waves. It is important both to understand the gasdynamics of the waveriders themselves and the ability to use them in hypersonic aircraft.

Note that, as a rule, numerical investigations are referred to the waveriders designed from conical flowfields, for example, Refs. 17–22. Planar shock waveriders have not been studied much in off-design flow regimes, excluding a caret wing. However, because of its geometric features, the caret wing unsuitable for designing of the hypersonic scramjet-powered vehicles. In Ref. 17, the data computed by Euler solver for the planar shock waverider with a sharp parabolic leading edge is presented only in the on-design regime at $M_\infty = M_d = 5.5$.

How can the viscosity affect the results obtained by the Euler simulation of the inviscid flowfields over waveriders? Comparison of the data for the conical shock sharp-edged waveriders obtained from solution of the Navier–Stokes and Euler equations is presented in Refs. 18 and 19. These data show that the viscous effects do not essentially affect the surface pressure distribution. The Euler and turbulent waveriders basically have the same pressure values, except in the tip vicinity. The same effects can be observed in the flowfield on the whole.

For high flight velocities, the problem of influence of rounding of the waverider leading edges necessary for decrease of their heating on the flow structure is considered.[20–22] Thus, at $M_\infty = 6$, the rounding of the leading edge to 0.01 m in radius had a negligible effect on the structure of the flowfield on the lower surface, as shown

Received 23 December 2002; revision received 21 April 2003; accepted for publication 23 April 2003.

*Senior Research Scientist, Experimental Aerodynamics Laboratory, Institute of Theoretical and Applied Mechanics.

†Research Scientist, Experimental Aerodynamics Laboratory, Institute of Theoretical and Applied Mechanics.

in Ref. 21. Investigations[22] at $M_\infty = 8$ determined that the disturbances generated by rounding are localized near the leading edge. The inviscid flowfield near most of the waverider actually remains unchanged.

For large Reynolds number conditions, a turbulent boundary layer, and moderate rounding of the leading edges, the indicated effects are not expected to be critical. Therefore, the principal features of the gasdynamic structure over the waveriders can be obtained from the Euler equations and with a configuration with sharp leading edges. Thus the regimes demanding further detailed analysis using more exact approaches can be revealed.

The investigation results of waveriders generated from the two-dimensional flow behind planar oblique shock waves are presented in this work. The body surface is analytically defined by the power-law functions[23–25] that allow one to obtain a wide range of cross sectional shapes including, for example, the widely known Nonweiler's caret wing.[1] This also enables one to conduct a parametric analysis and to search the efficient forms applicable to hypersonic aircraft. Under some conditions the waveriders considered can have an advantage in lift-to-drag ratio as compared with the conical ones.[25] The flow structure near the lower surface is numerically investigated by solution of the Euler equations. The off-design regimes at the freestream Mach numbers M_∞, which are larger and smaller than the design value M_d, are examined. The results presented are directed to investigations of the effect of cross-sectional shape, as well as to the capability to design waverider configurations that can be used as the basis for hypersonic scramjet-powered vehicles.

Definition of Waverider Surfaces

The geometry of the waveriders considered can be unambiguously determined if the transverse contour of the lower surface is known. To set the transverse contour, we use the power-law function

$$z_l = B(y_0 - y_l)^n \tag{1}$$

where $y_0 = -x \tan\delta$, $y_l < y_0$. The coordinate system and a general view of a waverider is shown in Fig. 1.

The leading edge is determined by intersection of the freestream streamlines with a shock wave plane that further passes through the assigned transverse contour of the lower surface. Thus, it is related to the transverse contour shape and shall also be described by a power-law function, which can be represented as

$$z_{\rm pl} = Ax^n \tag{2}$$

Equations (1) and (2) are not independent because to define the waveriders of the examined type it is sufficient to specify one of them. The relation between the coefficients A and B can be obtained using the condition that the leading edge should lie in the shock wave plane. This condition can be written as $y_{\rm pl} = -x \tan\beta$, where the vertical coordinate of the leading edge $y_{\rm pl}$ is determined from Eq. (1) at $z_l = z_{\rm pl}$. Thus, we have

$$B = A/(\tan\beta - \tan\delta)^n \tag{3}$$

Assuming that the upper surface is directed to the freestrem velocity vector and using the condition of angle inclination $\delta = {\rm const}$ for all cross sections $z = {\rm const}$ along a span, which is necessary for ensuring the on-design waverider regime, we can determine the upper surface. The correlation $y_u = y_l + \tan\delta(x - x_{\rm pl})$ results from this condition. Determining the coordinate of the leading edge $x_{\rm pl}$ in the section $z = {\rm const}$ from Eq. (2) and y_l from Eq. (1), we obtain $y_u = -(z/B)^{1/n} - \tan\delta(z/A)^{1/n}$. Then, using relation (3) for the description of the lower and upper surfaces in the accepted coordinate system, we have

$$y_l = -[x\tan\delta + (\tan\beta - \tan\delta)(z/A)^{1/n}]$$

$$y_u = -\tan\beta(z/A)^{1/n} \tag{4}$$

where $0 < x \le L$, $0 \le z \le z_{\rm pl}$, and $0 < n < \infty$.

In accord with Eq. (4), five independent parameters L, A, n, δ, and β (or the design Mach number M_d) will be assigned to determine the surface of the waveriders considered. The coefficient A can theoretically be varied within the limits $0 < A < \infty$. Its particular value can be chosen by setting the integral geometrical characteristics, such as volume, planform area, aspect ratio, etc., or the local characteristics of the leading edge, and the transverse contour (a sweep angle of the leading edges, inclination angles of the transverse contour in each cross section $x = {\rm const}$). The characteristics indicated are easily determined by Eqs. (2) and (4).[24,25] Here, the coefficient A is obtained by the aspect ratio of the configuration as $A = \lambda/[2(n+1)L^{n-1}]$.

Note some of the characteristic properties of the waveriders considered with varying the power-law exponent n. At $n = 1$, we have the waverider with rectilinear swept leading edges and the linear transverse contour of the surfaces, that is, Nonweiler's caret wing.[1] When $n > 1$, concave shapes of the leading edge in the planform, as well as the transverse contour, are observed, and when the power-law exponent is large, "narrow" configurations are realized. As a result of the geometry features, the configurations with $n \ge 1$ are not of practical interest. When n decreases, the leading edges and transverse contour become more convex, and within the limit of $n \to 0$, a nonswept rectilinear leading edge and waverider in the form of a wedge with side walls (cheeks) are obtained. Note that such configurations (with nonswept leading edges) will have increased drag at low supersonic and transonic velocities. Thus, investigations in the region of $0 < n < 1$ are the most desirable. At small n, the configurations with a sufficient planar section of the low surface transverse contour in the region of a plane of symmetry can be designed. This simplifies an integration problem of such waveriders, for example, with a flat inlet.

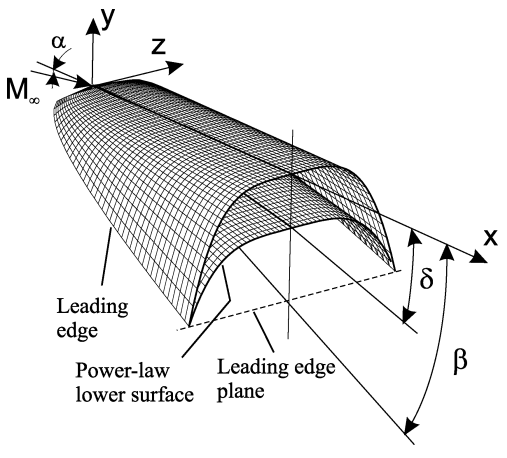

Fig. 1 General view of a waverider and coordinate system.

Calculation Method

Three-dimensional inviscid supersonic steady flow over waverider configurations in off-design regimes was investigated by the method of finite volumes using the algorithms of the numerical solution of the Euler equations described in detail in Refs. 26 and 27. The integration in the marching direction was performed using higher-order (up to third) explicit Runge–Kutta total variation diminishing schemes, which conserve the solution monotonicity and make it possible to capture gasdynamic discontinuities without introduction of artificial viscosity. The fluxes of the gasdynamic parameters on the sides between the computational cells were determined by solution of the supersonic flow interaction problem using the Harten–Laks–van–Leer–Einfeldt method. We use the third-order MUSCL method[28] for reconstructing the gasdynamic parameters on the cell sides from their volume-averaged values.

A multiblock approach was used to construct a computation grid. In the given case, the computational domain in each cross section was divided into three zones. Grid points on the boundaries between the neighboring zones were common, and the grids within different zones were generated completely independently. A number of grid

points in each computational cross section was 150×150, and a number of steps in the marching direction at integration up to the base section was about $5–7 \times 10^3$. The algorithm used allows one to separate the shock waves with smearing on 2–3 grid cells.

Any experimental investigations in the off-design regimes for the waveriders considered necessary for validation of the numerical solution are absent. An exception is the particular case when $n = 1$ (the Nonweiler's[1] caret wing). Correlation of the numerical and experimental data of the pressure coefficient obtained for the caret wings is shown in Fig. 2. In the case, where the boundary layer is not separated ($M_\infty = 4.04$ and $\alpha = 0.3$ deg), good convergence is observed for C_p level and position of the inner shock. At $M_\infty = 4.04$ and $\alpha = 8.2$ deg, boundary-layer separation is observed; however, agreement of the numerical and experimental data is found out of the separation region.

The other possible way to validate the numerical method used is obtaining data in the on-design regimes, where the exact solution is known. For the considered configurations, this way is more accessible and is not related to experimental errors. The shock wave lies in the leading-edge plane in such regimes, and the flow parameters near the waverider lower surface will be constant and equal to the parameters of the two-dimensional tangent wedge. Polars of the design regimes[29] of the waveriders studied are presented in Fig. 3. For example, for the configuration with $M_d = 6$ and $\delta = 5$ deg, the on-design regimes of the lower surface at $M_\infty = 6$ is found at $\alpha = 0$ and 15.4 deg; at $M_\infty = 8$, it is realized at $\alpha = 21.4$ deg. In the last case, the pressure values numerically obtained in the symmetry plane are $p/p_\infty = 23.7789$ at $\bar{x} = 0.1$ and 23.7523 at $\bar{x} = 1$; the analytical value for the corresponding two-dimensional flow is $p/p_\infty = 23.7981$. For the waverider with $M_d = 4$, and $\delta = 5$ deg, the design regime at $M_\infty = 4$ is realized for $\alpha = 0$ and 18 deg. At $\alpha = 18$ deg, the value $p/p_\infty = 6.2771$ is obtained at $\bar{x} = 0.1$ and 6.2755 at $\bar{x} = 1$; the analytical value is $p/p_\infty = 6.2774$. These data characterize the high accuracy of the three-dimensional numerical algorithm used. The flow patterns near the lower surface in the on-design regimes noted are also presented in Fig. 3 in the form of the equal relative density contours ρ/ρ_∞.

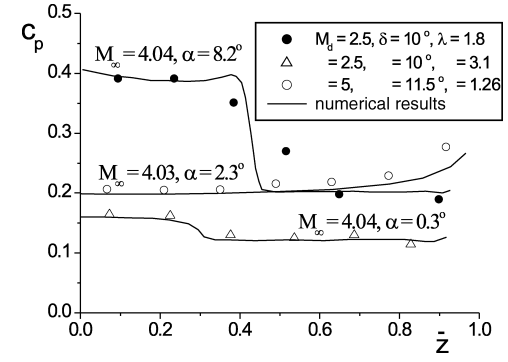

Fig. 2 Comparisons of numerical and experimental data for caret wings ($n = 1$).

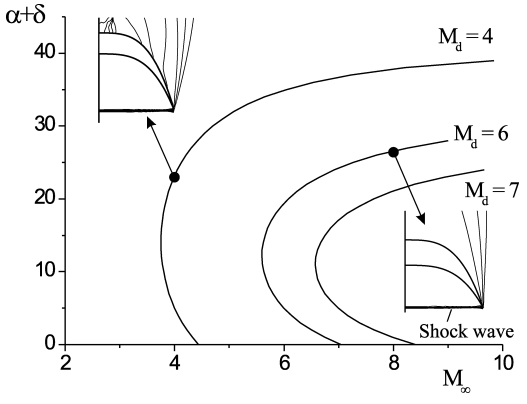

Fig. 3 Polars of the on-design regimes of the waveriders studied.

Numerical Results in the Off-Design Regimes

Numerical investigations of the flow patterns over the waveriders were performed at the freestream Mach numbers $M_\infty = 4$, 5, 6, 6.5, and 8. The data have been obtained for configurations with the design Mach numbers $M_d = 4$, 6, and 7, basic-wedge angle $\delta = 5$ deg, and aspect ratio $\lambda = 0.7$.

Flow Patterns over Waveriders of Different Shapes

The power-law exponent n is the main parameter determining a planform and cross-sectional shapes of waveriders studied. Consider the effect of this parameter on flow patterns near the lower surface in the off-design regimes $M_\infty > M_d$ using the configuration with $M_d = 6$ as an example.

Figure 4 shows the equal relative density contours in the base section $x = L$ for the configurations with different power-law exponents n at $M_\infty = 8$ and $\alpha = 0$. These data enable one to judge the change of the flow patterns over the differently shaped bodies. For the configurations at $n > 0.8$, the irregular interaction of the shock waves occurs, as for the known caret wings ($n = 1$). The following shock waves in the flow structure can be distinguished: the central shock, the shock attached to the leading edges, and, as a result of their interactions, an inner shock wave incident on the body surface. However, when the power-law exponent decreases in the region $n < 0.8$, a degeneration of the inner shock wave is realized. Therefore, the flow with one concave shock wave attached to the leading edges takes place.

The spanwise pressure distribution p/p_∞ on the lower surface in the cross section $x = L$ is presented in Fig. 5, which allows one to explain the flow details more exactly. The flow character in the region between the leading edges and the inner shock wave is different at various configurations with regard to $n \sim 1$. Thus, at $n = 1.25$, in this region flow expansion and pressure decrease in direction toward the body symmetry plane are observed, and at $n = 0.8$, flow

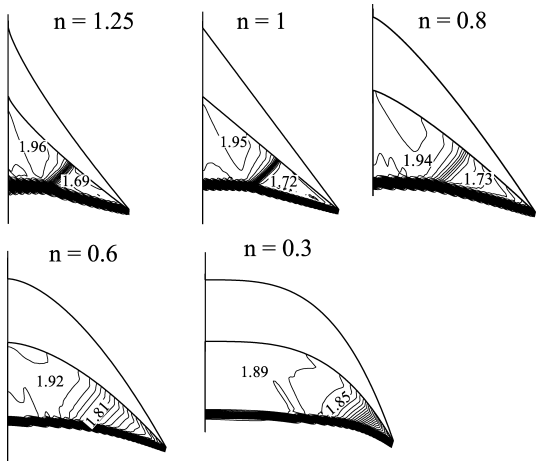

Fig. 4 Variation of the flow patterns in the cross sections $x = L$ depending on the power-law exponent n, $M_\infty = 8$, $\alpha = 0$, and $M_d = 6$.

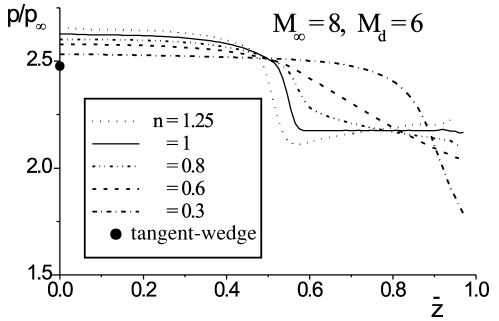

Fig. 5 Spanwise pressure distributions in the cross sections $x = L$ for the waveriders with different power-law exponents n.

compression is realized. This is related to the corresponding change of curvature sign of the lower surface transverse contour when crossing the point $n = 1$. At $n = 1.25$, higher pressure levels at the leading edges themselves and in the symmetry plane region are observed. However, the inner shock intensity is also higher in the last case, and it decreases with decreasing parameter n. The pressure level corresponding to the two-dimensional solution for the tangent wedge with the angle of $\alpha + \delta$ is also presented in Fig. 5.

When n decreases, the inner shock wave moves toward the leading edges and as noted, the wave degenerates. At $n \leq 0.6$, a smooth pressure increase to the plane of symmetry is observed. Thus, the negative pressure gradient toward the leading edges is realized for the crossflow. These gradients are favorable for decreasing boundary-layer thickness. Analysis of the boundary-layer characteristics[30] using the full Navier–Stokes equations show that the gradients of such types leads to the streamline deflection in the boundary layer toward the leading edges. Thus, spilling of the boundary layer from the body central part, that is, from the region of a possible location of the power plant, is realized.

Note that, for the configurations with $n \leq 0.3$, a sufficiently uniform pressure distribution and uniform flowfield between the surface and shock wave are observed in the largest span region of a body $0 \leq \bar{z} < 0.7$. Particularly, at $n = 0.3$, nonuniformity of the Mach number and pressure on the body in this region are 3.4 and 2.2%, respectively, and between the surface and shock wave in the plane of symmetry it is about 0.02 and 0.2%. When the lower surface is considered as a precompression surface for an engine inlet of advanced vehicles, the factor mentioned is favorable in combination with a sufficiently flat transverse contour of the lower surface of this region.

Development of the flow patterns with decreasing n coincides with an expected one for the limit case $n = 0$. At $n = 0$, as mentioned earlier, a waverider represents a wedge with side walls. In the on-design regime, the flow over such configuration has a two-dimensional character without inner shock waves and with the uniform parameter distribution near the whole lower surface. However, as compared with the configurations at $n > 0$, in spite of this advantage, a zero sweep of the leading edges will lead to increase of drag, especially at transonic flight velocities.

Because of the initial geometry, the flow near the considered configurations is not conical, excluding the variant at $n = 1$. The flow is determined by the variable values of sweep angle of the leading edge along the length and the inclination angle of the transverse contour of the lower surface at the leading edges. The flow patterns on the lower surface are presented in Fig. 6 by the equal density contours for the configurations with different power-law exponent. The inner shock wave can be observed along the full body length at $n = 1.25$. Its intensity is significantly weaker at $n = 0.8$, and at $n = 0.6$, it is absent.

Numerical calculations show that at $n = 1.25$ the shock wave intensity at the leading edge increases along the configuration length toward the base section (Fig. 7). This intensity growth is specified by increasing the velocity component normal to the leading edge due to the decrease in the sweep. Intensity of the inner shock wave decreases. Therefore, the inner shock wave is generated closer and

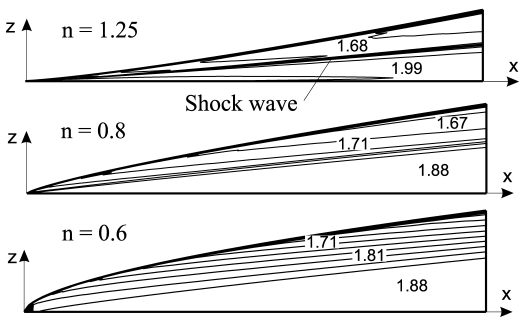

Fig. 6 Equal relative density contours on the lower surface of waveriders, $M_\infty = 8$, $\alpha = 0$.

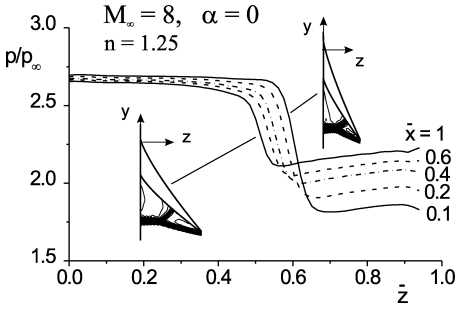

Fig. 7 Spanwise pressure distributions in different cross sections for the waverider with power-law exponent $n = 1.25$.

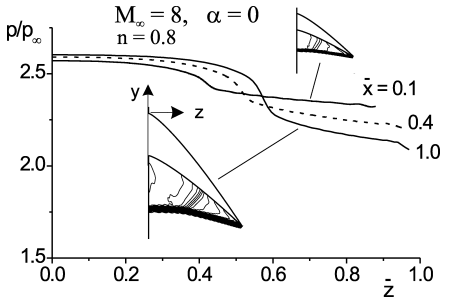

Fig. 8 Spanwise pressure distributions in different cross sections for the waverider with power-law exponent $n = 0.8$.

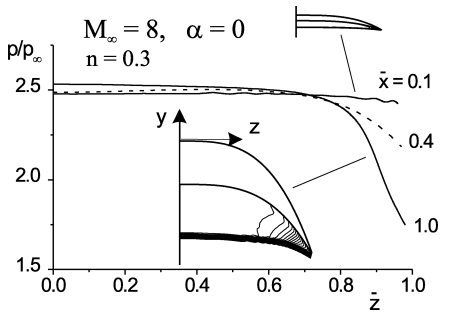

Fig. 9 Spanwise pressure distributions in different cross sections for the waverider with power-law exponent $n = 0.3$.

closer to the plane of symmetry with increase of the relative coordinate $\bar{x}$. In the region between the leading edge and inner shock wave, a decrease of the pressure is observed on the body surface for all values of $\bar{x}$, that is, a flow expansion takes place. The features indicated are also seen in Fig. 7, where the equal-density contours in the cross sections are demonstrated.

The other features occur when $n < 1$. Pressure distribution on the lower surface and equal-density contours in a set of the cross sections $\bar{x} = \text{const}$ are presented in Figs. 8 and 9. Thus, at $n = 0.8$ (Fig. 8), the pressure in the region of the leading edge reduces along the body length, that is, the shock wave intensity decreases at the leading edge. However, the intensity of the inner shock wave increases, and the shock moves toward the leading edge. In the region between the leading edge and inner shock wave, the pressure slightly increases, that is, compression flow occurs.

For the configuration with $n = 0.3$, there is no inner shock wave (Fig. 9). The compression flow whose intensity increases with increasing the coordinate $\bar{x}$ is observed behind the concave shock wave attached to the leading edge. Besides, at $n < 1$, the flow is compressed at its motion along the longitudinal coordinate unlike the configurations with $n > 1$, when a weak pressure decreases in the plane of symmetry $z = 0$ is observed with increasing $\bar{x}$ (Fig. 7). The pressure distribution in the region $0 \leq \bar{z} < 0.7$ is sufficiently uniform almost along whole lower surface.

Flow Patterns at Angles of Attack $\alpha > 0$

Based on the waverider configuration with $n = 0.3$ and $M_d = 6$, the flow structure change near the lower surface is considered vs angle of attack at $M_\infty = 8$. For small values of $\alpha \sim 0$, the flowfield's character is similar to that presented in Fig. 4. In this case, flow compression without the inner shock waves is observed in the leading-edge region. Calculations show that a smooth turning of the flow streamlines along the surface to the body symmetry plane is realized. With further increasing of α, such flow without the inner shock waves is not sufficient for turning in parallel to the plane of symmetry. By $\alpha \approx 3$ deg in the cross sections $x \sim L$, formations of inner shock wave and irregular interaction of shocks are observed near the leading edges.

Development of the flow pattern with increasing α is presented in Fig. 10, where the contours ρ/ρ_∞ are shown in the cross section $x = L$. Note the existence of a fan expansion starting from the point of a Mach interaction of the shock waves at $\alpha \geq 6$ deg. When it descends on the body surface, a wave expansion leads to pressure decrease. The on-design regime with one shock in the leading-edge plane will be realized at large angles of attack (Fig. 3, $M_d = 6$ and $M_\infty = 8$), that corresponds to two-dimensional flow near the lower waverider surface. In the given case, a design regime occurs at $\alpha = 21.4$ deg, and it is shown also in Fig. 10.

Figure 11 presents a spanwise pressure distribution in the cross section $x = L$. Note that the inner shock wave intensity increases with increasing angle of attack. Thus, for example, at $\alpha = 9$ deg, the pressure level in the inner shock wave reaches the value $p/p_\infty = 10.1$. That significantly exceeds the value $p/p_\infty = 8.36$ for the two-dimensional flow over tangent wedge with the angle $\delta + \alpha$. At large α, just immediately behind the inner shock wave, a sufficient sharp decrease of the pressure is observed that is caused by an expansion wave. With increase of the angle of attack, the inner shock moves toward the leading edge. Note that at $\bar{z} < 0.7 - 0.8$ the flow near the lower surface remains sufficiently uniform in the whole range of angles of attack investigated.

The initiation of the inner shock waves takes place first near the bottom section. However, when the angle of attack increases, the inner shock wave moves toward the body nose. This is shown in Fig. 12, where the flow patterns are presented in the form of equal density contours on the lower surface at $\alpha = 9$ deg.

The numerical data at the off-design Mach number $M_\infty = 8$ and large angles of attack show that a transfer from the flow with one concave shock wave at small α to the design regime with a planar shock wave at the leading edges at large α is realized by the irregular shock wave interactions and further displacement of the inner shock and the shock at the leading edges by a central one (Fig. 10).

Effect of Design Mach Number

Examples of the flow patterns considered referred to the configurations with the design Mach number $M_d = 6$. The value of M_d for a hypersonic aircraft, evidently, will be determined from the condition of a maximal efficiency of a cruising flight regime. Note that, according to Eq. (2), the planform remains the same at the given n and λ. Thus, waveriders with different M_d have equal sweep angles along the leading edge. However, the gasdynamic structure will be different because the value of M_d determines a position of the plane of the leading edges.

The relative density contours in the base section $x = L$ at $M_\infty = 8$, $\alpha = 0$, and $n = 0.3$ for the configurations with different values of the design Mach number M_d are presented in Fig. 13. At small deviations of the freestream Mach number with regard to M_d, a sufficiently uniform flowfield near the lower surface is realized. Increase of this deviation first leads to extension of the flow compression region near the leading edge ($M_d = 6$) and then to formation of the inner shock waves ($M_d = 4$).

Figure 14 shows a pressure distribution along the surface of the given configurations at $M_\infty = 8$ and $\alpha = 0$. The character of the

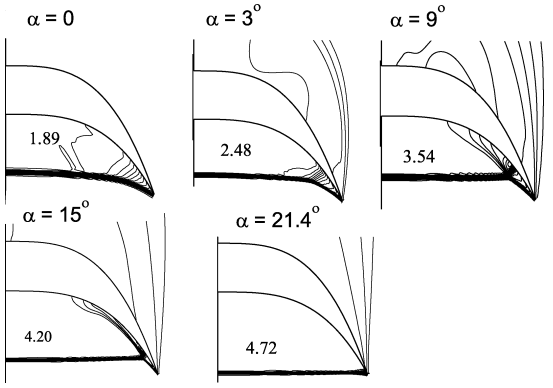

Fig. 10 Variation of flow patterns in cross sections $x = L$ vs angles of attack, $M_\infty = 8$ and $M_d = 6$.

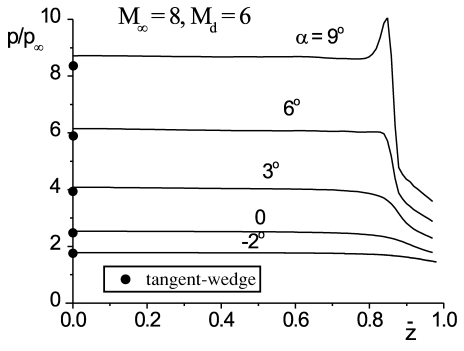

Fig. 11 Effects of angle of attack on the pressure distribution.

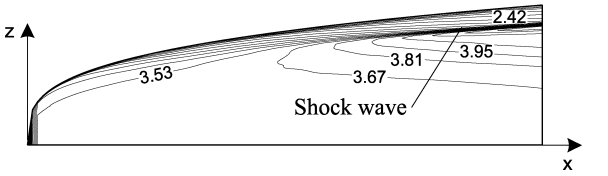

Fig. 12 Equal relative density contours at $\alpha = 9$ deg for waverider with power-law exponent $n = 0.3$, $M_\infty = 8$ and $M_d = 6$.

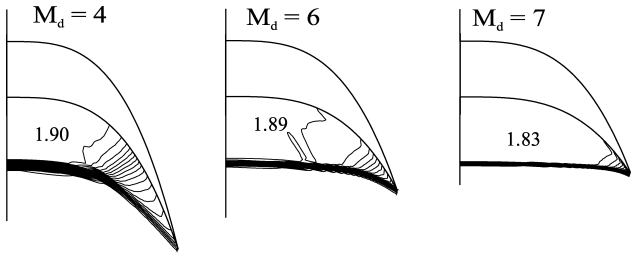

Fig. 13 Flow patterns in the cross sections $x = L$ for waveriders with different design Mach numbers, $M_\infty = 8$ and $\alpha = 0$.

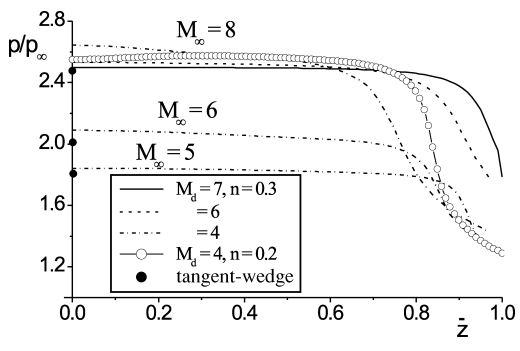

Fig. 14 Spanwise pressure distributions in the cross sections $x = L$ for waveriders with different design Mach numbers.

pressure distribution corresponds to the flow structure presented earlier. At small departure of M_∞ from M_d (where $M_d = 7$ and 6 in the given case), a practically uniform pressure distribution at the largest part of the span $\bar{z} < 0.7 - 0.8$ is observed. With decrease of M_d, the pressure straight in the leading-edge region is also decreased, and the flow nonuniformity is increased on the whole. A pressure level in the plane of symmetry increases and exceeds the pressure in a two-dimensional flow over tangent wedge; the corresponding values are shown in Fig. 14.

The effect of the freestream Mach number on the pressure distribution are presented in Fig. 14 for the configuration with $M_d = 4$. When M_∞ decreases and approaches the on-design regime, the region of sharp pressure change moves to the leading edge, and the uniform flow dominates near most of the surface.

To extend the uniform flow region on the lower surface at significant departures from the on-design regime $M_\infty > M_d$, it is necessary to choose lower values of the power-law exponent n. The values for the waverider with $M_d = 4$ and $n = 0.2$ are shown in Fig. 14 as an example. In this case, the movement of the region of a sharp pressure change toward the leading edges is observed as compared with the configuration with $n = 0.3$.

Flow Regimes with $M_\infty < M_d$

Let us consider the flow patterns of the configurations investigated in the regimes at $M_\infty < M_d$. There available data for the planar shock waveriders for the particular case with $n = 1$, that is, for the caret wings. A feature of the configurations with $n \neq 1$ is variable sweep of the leading edge along the body length. This has to lead to the fact that at $M_\infty < M_d$ the conditions of a shock wave detachment along the leading edges will be different, and so different flow regimes of the leading edges can occur.

First consider slight deviations from the on-design regime. The flow patterns based on the equal-density contours at $M_\infty = 6.5$ and $\alpha = 0$ are presented in Fig. 15 for the configuration with $M_d = 7$ and $n = 0.3$. According to the numerical calculations, a shock wave is attached to the leading edges up to the section $\bar{x} = 0.4$, and there are no disturbances on the upper surface. The detachment of shock wave takes place farther downstream; thus, even at $\bar{x} = 0.8$, an overflow to the upper surface is weak. The flowfield near the lower surface remains practically uniform. Moving away from the on-design regime, a point of the shock detachment on the leading edges moves toward the body tip. Thus, decrease of Mach number to $M_\infty = 6$ leads to motion of the detachment point to $\bar{x} = 0.2$. In spite of this, the pressure distribution on the body surface in the region $0 \leq \bar{z} < 0.8$ at all cross sections is practically uniform.

Another example is considered for the configuration with $M_d = 6$ and $n = 0.3$ at the freestream Mach number $M_\infty = 4$ and $\alpha = 0$–9 deg. This corresponds to significantly large deviations from the on-design regimes, shown in Fig. 3. According to the numerical calculations at $\alpha = 0$, the shock is attached to the leading edges for the values of the longitudinal coordinate $\bar{x} \leq 0.2$, and at higher $\bar{x}$, the shock is detached. With an increase of angle of attack, the point of the shock wave detachment slightly moves forward along the leading edge.

Figure 16 shows, as an example, the pressure distribution along the surface and the equal-density contours in a set of cross sections at $\alpha = 9$ deg. In the section at $\bar{x} = 0.1$, the shock wave is attached to the leading edge; at $\bar{x} = 0.2$, the shock begins to be detached, and the disturbances propagate into the upper surface region. The shock moves farther away from the leading edge when $\bar{x}$ increases, and

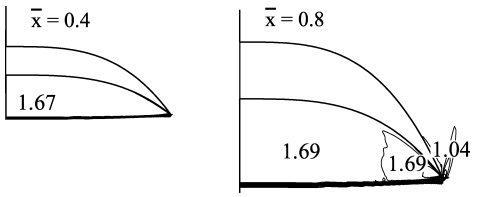

Fig. 15 Flow patterns in the cross sections of a waverider at $M_\infty < M_d$; $\alpha = 0$, $M_\infty = 6.5$, and $M_d = 7$.

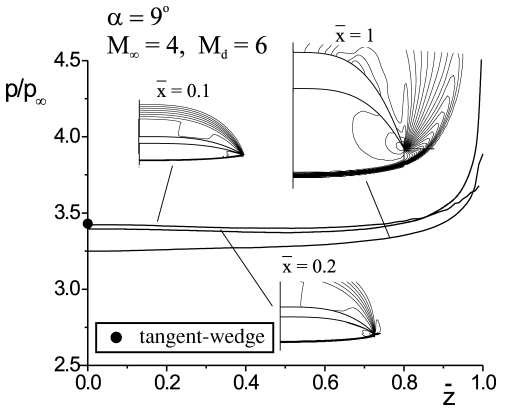

Fig. 16 Spanwise pressure distributions and flow patterns in the cross sections of a waverider at $M_\infty < M_d$.

flow spillage also increases. Therefore, bow shock angle decrease occurs in the plane of symmetry; it comes to ~3 deg along the full body length. A slight decrease in lengthwise pressure distribution is observed in the symmetry plane of the body, which is stronger at large angles of attack. For example, at $\alpha = 9$ deg for $\bar{x} = 0.1$ and 1, the values are $p/p_\infty = 3.42$ and 3.25, respectively, that is, the decrease is ~5%.

In the range investigated, $\alpha = -2$–9 deg, the pressure distribution on the body surface in all cross sections is practically uniform in the region $0 \leq \bar{z} < 0.8$; then, the pressure further increases to the leading edge. The pressure level at the two-dimensional tangent wedge with the angle $\delta + \alpha$ is $p/p_\infty = 3.43$; this point is also presented in Fig. 16. It is seen that the flow in the configuration initial sections in the region of the plane of symmetry under conditions considered is close to the two-dimensional flow.

Thus, for the configurations at $M_\infty < M_d$, the flow peculiarity related to different flow regimes at the leading edge is observed, both with the attached shock wave at small values of the relative longitudinal coordinate $\bar{x}$ and the detached shock wave at higher $\bar{x}$.

Conclusions

Results of the numerical simulation of the flow patterns over the waveriders designed based on the flow behind oblique shock waves are presented. The surface of such waveriders is described by the power-law functions.

The flow patterns of the waveriders with different shapes of cross section are studied in the off-design regimes by means of the Euler equations. The possibility to design the configurations flown at $M_\infty > M_d$ with one concave shock wave attached to the leading edges is shown. Thus, at $M_\infty = 8$ and $\alpha = 0$ for the waveriders with $M_d = 6$ degeneration of the inner shock wave and flow transition with irregular interaction of shock waves to the flow with one concave shock wave are observed in case of a power-law exponent decrease down to $n \sim 0.6$ and smaller. However, for configurations at $M_\infty > M_d$ and $\alpha > 0$, a transition to the on-design regime with planar shock wave at large angles of attack is realized by formation of shock irregular interactions with increase of α and further displacement of the inner shock and the shock at the leading edges by central shock.

For configurations with $n \leq 0.3$ at small α, the flowfield in the region $0 \leq \bar{z} \leq 0.7$–0.8 remains practically uniform for the both regimes at $M_\infty < M_d$ and $M_\infty > M_d$. This flow uniformity and a sufficient flat transverse contour in the region of the plane of symmetry are favorable factors for using such configurations as the basis of advanced hypersonic vehicles.

References

[1]Nonweiler, T. R. F., "Aerodynamic Problems of Manned Space Vehicles," *Journal of Royal Aeronautical Society*, Vol. 63, Sept. 1959, pp. 521–528.

[2]Maikapar, G. I., "On Construction of Supersonic Flows Around Solid Bodies with the Use of Planar Shocks," *Izvestiya AN SSSR, Mekhanika i Mashinostroenie*, No. 5, 1964, pp. 142–144 (in Russian).

[3]Collingbourne, J. R., and Peckham, D. H., "The Lift Drag Characteristics of Caret Wings at Mach Numbers Between 5 and 10," Aeronautical Research Council, CP-930, Ministry of Technology, Her Majestry's Stationary Office Press, London, 1967.

[4]Jones, J. G., and Woods, B. A., "The Design of Compression Surfaces for High Supersonic Speeds Using Conical Fields," Aeronautical Research Council, R&M 3539, Ministry of Technology, Her Majestry's Stationary Office Press, London, 1963.

[5]Kim, B. S., Rasmussen, M. L., and Jischke, M. C., "Optimization of Waverider Configurations Generated from Axisymmetric Conical Flows," *Journal of Spacecraft and Rockets*, Vol. 20, No. 5, 1983, pp. 461–469.

[6]Rasmussen, M. L., "Waverider Configurations Derived from Inclined Circular and Elliptic Cones," *Journal of Spacecraft and Rockets*, Vol. 17, No. 6, 1980, pp. 537–545.

[7]Cole, J. D., and Zien, T. F., "Class of Three-Dimensional Optimum Hypersonic Wings," *AIAA Journal*, Vol. 7, No. 2, 1969, pp. 264–271.

[8]Corda, S., and Anderson, J. D., "Viscous Optimized Hypersonic Waveriders Designed from Hypersonic Flow Fields," AIAA Paper 88-0369, Jan. 1988.

[9]Rasmussen, M. L., and Duncan, B., "Hypersonic Waveriders Generated from Power-Law Shocks," AIAA Paper 95-6160, April 1995.

[10]Goonko, Y. P., Mazhul, I. I., and Markelov, G. N., "Convergent-Flow-Derived Waveriders," *Journal of Aircraft*, Vol. 37, No. 4, 2000, pp. 647–654.

[11]McClinton, C. R., Voland, R. T., Holland, S. D., Engelund, W. C., White, J. T., and Pahle, J. W., "Wind Tunnel Testing, Flight Scaling and Flight Validation with Hyper-X," AIAA Paper 98-2866, June 1998.

[12]Haney, J. W., "A Waverider Derived Hypersonic X-Vehicle," AIAA Paper 95-6162, April 1995.

[13]Takashima, N., and Lewis, M. J., "Waverider Configuration Development for the Dual Fuel Vehicle," AIAA Paper 96-4593, 1996.

[14]Lewis, M. J., and Takashima, N., "Engine/Airframe Integration for Waverider Cruise Vehicles," AIAA Paper 93-0507, Jan. 1993.

[15]Blankson, I. M., and Haggseth, P., "Propulsion/Air-Frame Integration Issues for Waverider Aircraft," AIAA Paper 93-0506, Jan. 1993.

[16]Rudd, L., and Pines, D. J., "Dynamic Control of Mission Oriented Hypersonic Waveriders," AIAA Paper 99-4951, Nov. 1999.

[17]Jones, K. D., and Dougherty, F. C., "Numerical Simulation of High-Speed Flows About Waveriders with Sharp Leading Edges," *Journal of Spacecraft and Rockets*, Vol. 29, No. 5, 1992, pp. 661–667.

[18]Shi, Y., Tsai, B.-J., Miles, J. B., and Isaac, K. M., "Cone-Derived Waverider Flowfield Simulation Including Turbulence and Off-Design Conditions," *Journal of Spacecraft and Rockets*, Vol. 33, No. 2, 1996, pp. 185–190.

[19]Shi, Y., Miles, J. B., and Isaac, K. M., "Computational Fluid Dynamics Simulation of Turbulent Waverider Flowfield with Sideslip," *Journal of Spacecraft and Rockets*, Vol. 34, No. 1, 1997, pp. 76–82.

[20]Eggers, T., Radespiel, R., Waibel, M., and Hummel, D., "Flow Phenomena of Hypersonic Waveriders and Validation of Design Methods," AIAA Paper 93-5045, Nov. 1993.

[21]Takashima, N., and Lewis, M. J., "Navier–Stokes Computation of a Viscous Optimized Waverider," *Journal of Spacecraft and Rockets*, Vol. 31, No. 3, 1994, pp. 383–391.

[22]He, X., and Rasmussen, M. L., "Computational Analysis of Off-Design Waveriders," *Journal of Aircraft*, Vol. 31, No. 2, 1994, pp. 345–353.

[23]Shchepanovsky, V. A., "Construction of Hypersonic Flows over Three-Dimensional Configurations on the Basis of Two-Dimensional Flows," *Investigations in Hypersonic Aerodynamics*, Inst. of Theoretical and Applied Mechanics, Academy of Science of the USSR Press, Siberian Branch, Novosibirsk, Russia, 1978, pp. 34–50 (in Russian).

[24]Starkey, R. P., and Lewis, M. J., "Analytical Off-Design Lift-to-Drag-Ratio Analysis for Hypersonic Waveriders," *Journal of Spacecraft and Rockets*, Vol. 37, No. 5, 2000, pp. 684–691.

[25]Mazhul, I. I., "Waveriders with Power-Law Transverse Contour of Lower Surface," *Thermophysics and Aeromechanics*, Vol. 9, No. 1, 2002, pp. 85–98.

[26]Kudryavtsev, A. N., and Rakhimov, R. D., "A Marching Procedure of Numerical Solution of Two-Dimensional and Three-Dimensional Steady Euler Equations Using Shock-Capturing Schemes," *Proceedings of International Conference on the Methods of Aerophysical Research*, Pt. 1, Inst. of Theoretical and Applied Mechanics, Russian Academy of Science Press, Siberian Branch, Novosibirsk, Russia, 1998, pp. 117–122.

[27]Goonko, Y. P., Kharitonov, A. M., Kudryavtsev, A. N., Mazhul, I. I., and Rakhimov, R. D., "Euler Simulations of the Flow over a Hypersonic Convergent Inlet Integrated with a Forebody Compression Surface," *Proceedings of European Congress on Computational Methods in Applied Science and Engineering* [CD-ROM], Barcelona, Sept. 2000.

[28]Anderson, W. K., Thomas, J. L., and van Leer, B., "Comparison of Finite Volume Flux Vector Splitting for the Euler Equations," *AIAA Journal*, Vol. 24, No. 9, 1986, pp. 1453–1460.

[29]Venn, J., and Flower, J. W., "Shock Patterns for Simple Caret Wings," *Aeronautical Journal*, Vol. 74, No. 712, 1970, pp. 339–348.

[30]Gubanov, A. A., and Takhovitsky, S. A., "Investigation on a Choice of a Planform of Lifting Surface Applied as a Precompression One for an Inlet with Taking into Account the Boundary Layer Forming on It," *Basic Research for Hypersonic Technologies*, Vol. 2, Central Aerohydrodynamic Institute (TsAGI) Press, Zhukovsky, Russia, 1998, pp. 88–97 (in Russian).